

New Development of Bayesian Variable Selection Criteria for Spatial Point Process with Applications

Guanyu Hu *, Fred Huffer, and Ming-Hui Chen

Abstract

Selecting important spatial-dependent variables under the nonhomogeneous spatial Poisson process model is an important topic of great current interest. In this paper, we use the Deviance Information Criterion (DIC) and Logarithm of the Pseudo Marginal Likelihood (LPML) for Bayesian variable selection under the nonhomogeneous spatial Poisson process model. We further derive the new Monte Carlo estimation formula for LPML in the spatial Poisson process setting. Extensive simulation studies are carried out to evaluate the empirical performance of the proposed criteria. The proposed methodology is further applied to the analysis of two large data sets, the Earthquake Hazards Program of United States Geological Survey (USGS) earthquake data and the Forest of Barro Colorado Island (BCI) data.

Keywords: BCI Data, DIC, LPML, Monte Carlo Estimation, USGS Earthquake Data

1 Introduction

There are three different types of spatial data, including point-reference data, areal data, and spatial point pattern data. Spatial point pattern data are the random locations of events in space (Cressie, 1993; Banerjee, Carlin, & Gelfand, 2014). Spatial point patterns assume

*(to whom correspondence should be addressed) Email: guanyu.hu@uconn.edu Department of Statistics, University of Connecticut.

the randomness is associated with the locations of the points. Spatial point process models have been developed for analyzing spatial point pattern data (Møller & Waagepetersen, 2003; Diggle, 2013). Spatial point pattern data are routinely encountered in many different fields such as seismology, ecology, environmental science, and epidemiology. A common goal of these fields is to connect spatially dependent covariates to the occurrence of events of interest in space. Spatial point process regression models are well-suited for this goal. Spatial Poisson point processes are widely used for the purpose of regression analysis due to the easy implementation and the attractive theoretical properties.

For regression problem, variable selection methods are widely studied in the statistical literature. The information criterion based variable selection methods such as [Akaike information criterion](#) (AIC) (Akaike, 1974) or [Bayesian information criterion](#) (BIC) (Schwarz et al., 1978) are easy to implement. Other than the information criterion based methods, the regularized regression methods such as ridge regression (Hoerl & Kennard, 1970), LASSO (Tibshirani, 1996), and elastic net (Zou & Hastie, 2005) are also important tools for variable selection. Within the Bayesian framework, the deviance information criterion (DIC) (Spiegelhalter, Best, Carlin, & Van Der Linde, 2002) and the logarithm of the pseudo marginal likelihood (LPML) (Gelfand & Dey, 1994) are two popular model selection assessment criteria. Priors based approaches (spike and slab prior (Ishwaran, Rao, et al., 2005) and shrinkage prior (Polson & Scott, 2010)) are also developed for Bayesian variable selection.

In the existing literature, the variable selection problem has been extensively studied for point-reference data or areal data ((Wang & Zhu, 2009; Reich, Fuentes, Herring, & Evenson, 2010; Beale, Lennon, Yearsley, Brewer, & Elston, 2010)). However, for the spatial point process model, the literature on variable selection is relatively sparse. (Thurman & Zhu, 2014) proposed a regularized method that allows the selection of covariates at multiple pixel resolutions. (Yue & Loh, 2015) incorporated [least absolute shrinkage and selection operator](#) (LASSO), adaptive LASSO and elastic net regularization methods into the generalized linear model framework to select important covariates for spatial point process models. (Thurman, Fu, Guan, & Zhu, 2015) proposed a regularized estimating equation approach for the spatial point process model. (Leininger, Gelfand, et al., 2017) proposed Bayesian model assessment methods using the predictive mean square error, empirical coverage, and ranked probability

scores. But these methods do not account for the tradeoff between the goodness of fit and the model complexity.

The major contribution of this paper is to develop a novel implementation of DIC and LPML under spatial point process models. Compared with point-reference data, the traditional Monte Carlo method for computing Conditional Predictive Ordinate CPO (Chen, Shao, & Ibrahim, 2012) is not applicable for spatial point pattern data. Therefore, we develop a new Monte Carlo method of CPO for spatial point pattern data. Compared with the regularized methods, it is easy to carry out Bayesian inference using posterior samples based on our model selection approach. Our simulation studies show the promising empirical performance of the proposed Bayesian estimate criteria. In addition, our proposed Bayesian approach reveals some interesting features of the earthquake data sets. Furthermore, our proposed criteria overcome the limitations of regularized methods in selecting the important covariates and pixel resolution of the covariates simultaneously for BCI data.

The rest of this paper is organized as follows. In Section 2, we review nonhomogeneous spatial Poisson process and provide the Bayesian formulation of the spatial Poisson process model. The detailed development of DIC and LPML for the spatial Poisson process model is given in Section 3. Simulation studies are presented in Section 4. In Section 5, we carry out an in-depth analysis of the two data sets, the Earthquake Hazards Program of United States Geological Survey (USGS) earthquake data and Forest of Barro Colorado Island (BCI) data. We conclude the paper with a brief discussion in Section 6.

2 Bayesian Spatial Point Process

A spatial point pattern is a data set $\mathbf{y} = (s_1, s_2, \dots, s_\ell)$ consists the locations $(s_1, s_2, \dots, s_\ell)$ of points that are observed in a bounded region $\mathcal{B} \subseteq \mathcal{R}^2$, which is a realization of spatial point process \mathbf{Y} . $N_{\mathbf{Y}}(A) = \sum_{i=1}^{\ell} 1(s_i \in A)$ is a counting process associated with the spatial point process \mathbf{Y} , which counts the number of points of \mathbf{Y} for area $A \subseteq \mathcal{B}$. For the process \mathbf{Y} , there are many parametric distributions for a finite set of count variables like Poisson processes, Gibbs processes, and Cox processes. In this paper, our focus is on Poisson processes. For the Poisson process \mathbf{Y} over \mathcal{B} , which has the intensity function $\lambda(\mathbf{s})$, $N_{\mathbf{Y}}(A) \sim Po(\lambda(A))$, where

$\lambda(A) = \int_A \lambda(s)ds$. In addition, if A_1 and A_2 are disjoint, then $N_{\mathbf{Y}}(A_1)$ and $N_{\mathbf{Y}}(A_2)$ are independent, where $A_1 \subseteq \mathcal{B}$ and $A_2 \subseteq \mathcal{B}$. Based on the properties of the Poisson process, it is easy to obtain $E(N_{\mathbf{Y}}(A)) = \text{Var}(N_{\mathbf{Y}}(A)) = \lambda(A)$. When $\lambda(s) = \lambda$, we have the constant intensity over the space \mathcal{B} and in this special case, \mathbf{Y} reduces to a homogeneous Poisson process (HPP). For a more general case, $\lambda(s)$ can be spatially varying, which leads to a nonhomogeneous Poisson process (NHPP). For the NHPP, the log-likelihood on \mathcal{B} is given by

$$\ell = \sum_{i=1}^k \log \lambda(s_i) - \int_{\mathcal{B}} \lambda(s)ds, \quad (1)$$

where $\lambda(s_i)$ is the intensity function for location s_i . To build up a spatially varying intensity, $\lambda(s_i)$ is often assumed to take the following regression form:

$$\lambda(s_i) = \lambda_0 \exp(\boldsymbol{\beta} \mathbf{Z}(s_i)), \quad (2)$$

where λ_0 is the baseline intensity function, $\boldsymbol{\beta}$ is the vector of regression coefficient, and $\mathbf{Z}(s_i)$ is the vector of spatially varying covariates on location s_i .

For the model defined in (1) and (2), a gamma distribution for λ_0 is a conjugate prior. For the regression coefficients $\boldsymbol{\beta}$, there are no such conjugate priors for the log-likelihood in (1). We specify a non-informative normal prior for $\boldsymbol{\beta}$. Plugging (2) in (1) and using the above priors for λ_0 and $\boldsymbol{\beta}$, we have

$$\begin{aligned} \ell &= \sum_{i=1}^k (\log \lambda_0 + \boldsymbol{\beta} \mathbf{Z}(s_i)) - \int_{\mathcal{B}} \lambda_0 \exp(\boldsymbol{\beta} \mathbf{Z}(s))ds, \\ \lambda_0 &\sim \text{G}(a_1, b_1), \\ \boldsymbol{\beta} &\sim \text{MVN}(0, \sigma_0^2 I), \end{aligned} \quad (3)$$

where ℓ is the log-likelihood, and “G”, “MVN”, and “IG” are the shorthand of gamma distribution, multivariate normal distribution, and the inverse gamma distribution, respectively. Thus, the posterior distribution of $\boldsymbol{\theta} = (\lambda_0, \beta_1, \dots, \beta_p)$ is given as follow

$$\prod_{i=1}^n \lambda(s_i) \times \exp \left(- \int_{\mathcal{B}} \lambda(s)ds \right) \times \pi(\boldsymbol{\theta}), \quad (4)$$

where $\pi(\boldsymbol{\theta}) = \pi(\boldsymbol{\beta})\pi(\lambda_0)$ is the joint prior. The analytical evaluation of the posterior distribution of $\boldsymbol{\theta}$ is not possible. However, a Metropolis-Hasting algorithm within the Gibbs

sampler can be developed to sample from the posterior distribution in (4). The algorithm requires sampling the following parameters in turn from their respective full conditional distributions:

$$\begin{aligned} f(\boldsymbol{\beta}|\cdot) &\propto L \times \prod_{k=1}^p \frac{1}{\sqrt{2\pi\sigma_0^2}} \exp\left(-\frac{\beta_k^2}{2\sigma_0^2}\right), \\ f(\lambda_0|\cdot) &\propto L \times \frac{1}{\Gamma(a_1)b_1^{a_1}} \lambda_0^{a_1-1} \exp\left(-\frac{\lambda_0}{b_1}\right). \end{aligned} \quad (5)$$

We choose $\sigma_0^2 = 100$ and $a_1 = b_1 = 0.01$, while yields a non-informative joint prior for $\boldsymbol{\theta}$. To sample from the posterior distribution of $\boldsymbol{\theta}$ in (4), an Metropolis–Hasting within Gibbs algorithm is facilitated by R package `nimble` (de Valpine et al., 2017). The loglikelihood function of the spatial Poisson point process model used in the MCMC iteration is directly defined using the `RW_IIFunction()` sampler.

3 Bayesian Criteria for Variable Selection

We first introduce two Bayesian model selection criteria, Deviance Information Criterion (DIC) and logarithm of the Pseudo-marginal likelihood (LPML). The deviance information criterion is defined as

$$\text{DIC} = \text{Dev}(\bar{\boldsymbol{\theta}}) + 2p_D, \quad (6)$$

where $\text{Dev}(\bar{\boldsymbol{\theta}})$ is the deviance function, $p_D = \overline{\text{Dev}}(\boldsymbol{\theta}) - \text{Dev}(\bar{\boldsymbol{\theta}})$ is the effective number of model parameters, $\bar{\boldsymbol{\theta}}$ is the posterior mean of parameters $\boldsymbol{\theta}$, and $\overline{\text{Dev}}(\boldsymbol{\theta})$ is the posterior mean of $\text{Dev}(\boldsymbol{\theta})$.

The LPML is defined as

$$\text{LPML} = \sum_{i=1}^n \log(\text{CPO}_i), \quad (7)$$

where CPO_i is the conditional predictive ordinate (CPO) for the i -th subject. CPO is based on the leave-one-out-cross-validation. CPO estimates the probability of observing y_i in the future after having already observed $y_1, \dots, y_{i-1}, y_{i+1}, \dots, y_n$. The CPO for the i -th subject is defined as

$$\text{CPO}_i = f(y_i|\mathbf{y}_{-i}) \equiv \int f(y_i|\boldsymbol{\theta})\pi(\boldsymbol{\theta}|\mathbf{y}_{(-i)})d\boldsymbol{\theta}, \quad (8)$$

where \mathbf{y}_{-i} is $y_1, \dots, y_{i-1}, y_{i+1}, \dots, y_n$,

$$\pi(\boldsymbol{\theta}|\mathbf{y}_{-i}) = \frac{\prod_{j \neq i} f(y_j|\boldsymbol{\theta})\pi(\boldsymbol{\theta})}{c(\mathbf{y}_{-i})}, \quad (9)$$

and $c(\mathbf{y}_{-i})$ is the normalizing constant. The CPO_i in (8) can be expressed as

$$\text{CPO}_i^{-1} = \frac{1}{\int \frac{1}{f(y_i|\boldsymbol{\theta})}\pi(\boldsymbol{\theta}|\mathbf{y})d\boldsymbol{\theta}}. \quad (10)$$

Using (10), a Monte Carlo estimate of CPO_i in (10) is given by

$$\widehat{\text{CPO}}_i^{-1} = \frac{1}{B} \sum_{b=1}^B \frac{1}{f(y_i|\boldsymbol{\theta}_b)}, \quad (11)$$

where $\boldsymbol{\theta}_b$ is the b -th MCMC sample of $\boldsymbol{\theta}$ from $\pi(\boldsymbol{\theta}|\mathbf{y})$.

In the context of variable selection, we select a variable subset model which has the smallest DIC and the largest LPML.

3.1 DIC for Spatial Point Process

Since our main objective is to assess the fit of the spatial point pattern, we specify the following deviance function

$$\text{Dev}(D, \mathbf{Z}, \boldsymbol{\beta}, \lambda_0) = -2 \times \left(\sum_{i=1}^k \log \lambda(s_i) - \int_{\mathcal{B}} \lambda(s) ds \right), \quad (12)$$

where $D = (\mathbf{s}_1, \mathbf{s}_2, \dots, \mathbf{s}_k)$ is the observed points, $\lambda(s) = \lambda_0 \exp(\beta_1 Z_1(s) + \dots + \beta_p Z_p(s))$ is the intensity function on location \mathbf{s} , and $Z_1(s), Z_2(s), \dots, Z_p(s)$ are spatial covariates. Therefore, the DIC for the spatial point pattern is given as follows

$$\text{DIC} = 2E[\text{Dev}(D, \mathbf{Z}, \boldsymbol{\beta}, \lambda_0)] - \text{Dev}(D, \mathbf{Z}, \hat{\boldsymbol{\beta}}, \hat{\lambda}_0), \quad (13)$$

where $\hat{\boldsymbol{\beta}}$ and $\hat{\lambda}_0$ are the posterior means of $\boldsymbol{\beta}$ and λ_0 and the expectation is taken with respect to the posterior distribution of $\boldsymbol{\beta}$ and λ_0 .

3.2 LPML for Spatial Point Processes

In this section we propose a definition of LPML which is suitable for general Poisson processes. This definition is derived from the definition of LPML in (7) by a limiting argument.

We begin by slightly altering the definition of CPO_i given in (8). Let f_0 denote a fixed reference model for the data $\mathbf{y} = (y_1, y_2, \dots, y_n)$, and define

$$\text{CPO}_i = \frac{f(y_i|\mathbf{y}_{-i})}{f_0(y_i|\mathbf{y}_{-i})}. \quad (14)$$

This definition is essentially equivalent to that in (8) since the reference model cancels out when comparisons are made between models using $\text{LPML} = \sum_{i=1}^n \log(\text{CPO}_i)$. We shall assume that the reference model f_0 involves no parameters (or that any parameters are kept fixed at specified default values) and that the observations y_1, y_2, \dots, y_n are independent. In this case $f_0(y_i|\mathbf{y}_{-i}) = f_0(y_i)$. Repeating the argument which leads to (10) then yields

$$\text{CPO}_i^{-1} = \int \frac{f_0(y_i)}{f(y_i|\boldsymbol{\theta})} \pi(\boldsymbol{\theta}|\mathbf{y}) d\boldsymbol{\theta}. \quad (15)$$

Suppose we have a full Bayesian model (such as that described in (2) and (3)) for a Poisson process \mathbf{Y} with intensity $\lambda_{\boldsymbol{\theta}}(\cdot)$ on a region $\mathcal{B} \subset \mathcal{R}^2$. We observe the realization $Y = \{s_1, s_2, \dots, s_k\}$.

Let A_1, A_2, \dots, A_n be a partition of \mathcal{B} , i.e., disjoint subsets such that $\bigcup_{i=1}^n A_i = \mathcal{B}$. Suppose we were to make inference on $\boldsymbol{\theta}$ based only on the counts $(N_{\mathbf{Y}}(A_1), N_{\mathbf{Y}}(A_2), \dots, N_{\mathbf{Y}}(A_n))$ where $N_{\mathbf{Y}}(A_i) = \sum_{j=1}^k 1(s_j \in A_i)$. Conditional on $\boldsymbol{\theta}$, these counts are independent Poisson random variables which we take to be the values y_1, y_2, \dots, y_n making up the data \mathbf{y} in the generic notation of equations (14) and (15). For our reference model we use the Poisson process with a constant intensity of one. With these choices, we make the following substitutions in (15):

$$\begin{aligned} f(y_i|\boldsymbol{\theta}) &= \frac{\lambda(A_i)^{N_{\mathbf{Y}}(A_i)}}{N_{\mathbf{Y}}(A_i)!} \exp\{-\lambda(A_i)\}, \\ f_0(y_i) &= \frac{|A_i|^{N_{\mathbf{Y}}(A_i)}}{N_{\mathbf{Y}}(A_i)!} \exp(-|A_i|), \end{aligned}$$

where $\lambda(A_i) = \int_{A_i} \lambda(u) du$ and $|A_i| = \int_{A_i} du$. (Here, to lighten the notation, we omit the dependence of λ on $\boldsymbol{\theta}$.) Therefore

$$\frac{f_0(y_i)}{f(y_i|\boldsymbol{\theta})} = \left(\frac{\lambda(A_i)}{|A_i|} \right)^{-N_{\mathbf{Y}}(A_i)} \exp(\lambda(A_i) - |A_i|),$$

and we may write (15) as

$$\text{CPO}_i^{-1} = E_n \left[\left(\frac{\lambda(A_i)}{|A_i|} \right)^{-N_{\mathbf{Y}}(A_i)} \exp\{\lambda(A_i) - |A_i|\} \right],$$

where E_n represents the expectation over the posterior distribution of $\boldsymbol{\theta}$ given $(N_{\mathbf{Y}}(A_1), \dots, N_{\mathbf{Y}}(A_n))$.

For the fixed realization of the Poisson process $\mathbf{Y} = \{s_1, s_2, \dots, s_k\}$, we consider (informally) taking a limit as the partition A_1, A_2, \dots, A_n becomes progressively finer. When the partition is sufficiently fine, no set A_i will contain more than one of the points s_j ; exactly k of the sets A_i will contain one point, and the others will contain zero points. When the set A_i is sufficiently small, we expect $e^{\lambda(A_i) - |A_i|} \approx 1 + (\lambda(A_i) - |A_i|)$. Therefore, when all the sets $|A_i|$ are sufficiently small, for those sets A_i which contain zero points of \mathbf{Y} , we expect that

$$\text{CPO}_i^{-1} = E_n [\exp\{\lambda(A_i) - |A_i|\}] \approx 1 + E_n(\lambda(A_i) - |A_i|),$$

and based on the first order of Taylor expansion of $\log(1 + x)$, we have

$$\log \text{CPO}_i \approx -E_n(\lambda(A_i) - |A_i|). \quad (16)$$

If a set A_i is sufficiently small and contains a single point s_j of \mathbf{Y} , then (assuming the intensity $\lambda(u)$ is a continuous function of u for all $\boldsymbol{\theta}$) and A_i is smaller enough such that have negligible area) we expect $\lambda(A_i)/|A_i| \approx \lambda(s_j)$ and therefore

$$\text{CPO}_i^{-1} = E_n \left[\left(\frac{\lambda(A_i)}{|A_i|} \right)^{-1} e^{\lambda(A_i) - |A_i|} \right] \approx E_n \lambda(s_j)^{-1} (1 + (\lambda(A_i) - |A_i|)) \approx E_n [\lambda(s_j)^{-1}],$$

and

$$\log \text{CPO}_i \approx \log (E_n [\lambda(s_j)^{-1}])^{-1}. \quad (17)$$

Combining (16) and (17), we obtain

$$\begin{aligned} \text{LPML}_n &= \sum_{i=1}^n \log \text{CPO}_i = \sum_{i: N_{\mathbf{Y}}(A_i)=1} \log \text{CPO}_i + \sum_{i: N_{\mathbf{Y}}(A_i)=0} \log \text{CPO}_i \\ &\approx \sum_{j=1}^k \log (E_n [\lambda(s_j)^{-1}])^{-1} - \sum_{i: N_{\mathbf{Y}}(A_i)=0} E_n(\lambda(A_i) - |A_i|) \\ &\approx \sum_{j=1}^k \log (E_n [\lambda(s_j)^{-1}])^{-1} - \int_{\mathcal{B}} E_n[\lambda(u)] du + |\mathcal{B}|. \end{aligned}$$

As the partition gets progressively finer, the posterior conditional on the counts $(N_{\mathbf{Y}}(A_1), N_{\mathbf{Y}}(A_2), \dots, N_{\mathbf{Y}}(A_n))$ converges to the posterior conditional on the complete data \mathbf{Y} (Waagepetersen,

2004), and the various approximations we had made above become exact in the limit. We obtain

$$\lim_{n \rightarrow \infty} \text{LPML}_n = \sum_{j=1}^k \log (E [\lambda(s_j)^{-1}])^{-1} - \int_{\mathcal{B}} E[\lambda(u)] du + |\mathcal{B}|,$$

where E denotes the posterior expectation. Dropping the constant term $|\mathcal{B}|$, we take the remainder of this expression as our definition of the LPML for Poisson processes:

$$\text{LPML} = \sum_{j=1}^k \log (E [\lambda(s_j)^{-1}])^{-1} - \int_{\mathcal{B}} E[\lambda(u)] du, \quad (18)$$

where $\mathbf{Y} = \{s_1, s_2, \dots, s_k\}$ and E denotes the posterior expectation. There is a natural Monte Carlo estimate of the LPML given by

$$\widehat{\text{LPML}} = \sum_{j=1}^k \log \tilde{\lambda}(s_j) - \int_{\mathcal{B}} \bar{\lambda}(u) du, \quad (19)$$

where $\tilde{\lambda}(s_j) = (\frac{1}{B} \sum_{b=1}^B \lambda(s_j | \boldsymbol{\theta}_b)^{-1})^{-1}$, $\bar{\lambda}(u) = \frac{1}{B} \sum_{b=1}^B \lambda(u | \boldsymbol{\theta}_b)$, and $\{\theta_1, \theta_2, \dots, \theta_B\}$ is a sample from the posterior.

4 Simulation Study

In this section, we have four scenarios to generate covariates. The intensity function of data generation model (DGM) in scenario 1 is $\lambda(s) = \lambda_0 \exp(\beta_1 \times Z_1(s) + \beta_2 \times Z_2(s) + \beta_3 \times Z_1(s)Z_2(s))$, where $Z_1(s)$ and $Z_2(s)$ are x -coordinate and y -coordinate of location s . In this simulation we choose $\beta_1 = 2$, $\beta_2 = 0$, $\beta_3 = 1$, and $\lambda_0 = 30$ and generate data on $[0, 1] \times [0, 1]$. We generate 100 data sets under this setting, and the average number of points in this scenario is around 130. In this simulation study, we compare seven different models. We give $N(0, 10^2)$ prior on β s and $G(1, 1)$ prior on λ_0 . For each replicates, 20,000 MCMC samples are drawn and last 10,000 samples are kept for Bayesian inference. The full regression model includes x -coordinate, y -coordinate and their cross effects. The average DIC and LPML values and the selection percentage and model informations are shown in Table 1. This table indicates that (i) the true model has the smallest average DIC value and the largest average LPML value; (ii) the true model also has the largest selection percentages under both DIC and LPML; and (iii) Model 4 has the second smallest DIC value, the second

largest LPML value, and the second largest selection percentages. A partial explanation for (iii) is that both $Z_1(s)$ and $Z_2(s)$ are correlated with the interaction term $Z_1(s)Z_2(s)$.

Table 1: Selection Results of Scenario 1

Model	Average DIC	Average LPML	DIC Selection %	LPML Selection %
Model 1 (β_1)	-1147.300	573.639	12	12
Model 2 (β_2)	-1093.641	546.810	0	0
Model 3 (β_3)	-1133.599	566.790	0	0
Model 4 (β_1, β_2)	-1151.719	575.840	24	25
DGM (β_1, β_3)	-1152.609	576.284	53	52
Model 5 (β_2, β_3)	-1145.189	572.573	5	5
Model 6 ($\beta_1, \beta_2, \beta_3$)	-1151.656	575.788	6	6

Furthermore, we also show the boxplots of the DIC difference and the LPML difference between the true model and each of the candidate models in Figure 1. The medians and the inter quartile ranges (IQRs) of the DIC differences and the LPML differences are show in Table 2 Except for Models 4 the first quartiles of DIC differences are above 0 while the third

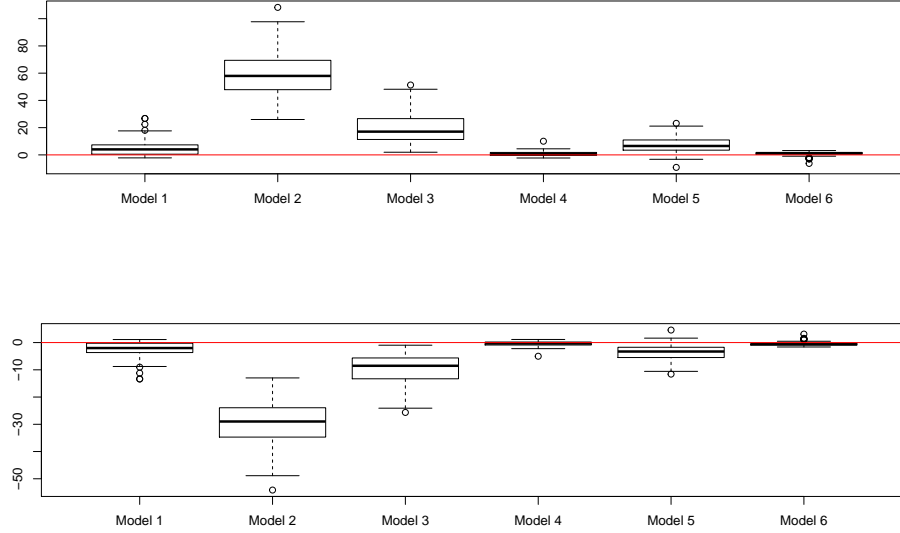
Table 2: Median and inter quartile ranges (IQRs) of the DIC and the LPML differences for Scenario 1

	DIC	LPML
Model 1	4.033 (0.517,7.339)	-2.009 (-0.253, -3.654)
Model 2	57.98 (48.03,69.35)	-28.97 (-24.00, -34.66)
Model 3	17.07 (11.60,26.40)	-8.520 (-5.789, -13.18)
Model 4	0.658 (-0.378,1.798)	-0.339 (0.197, -0.887)
Model 5	6.541 (3.48,10.95)	-3.281 (-1.735, -5.481)
Model 6	1.244 (0.576,1.771)	-0.635 (-0.298, -0.908)

quartiles of the LPML difference are below 0, which indicate that the true model outperform models 1, 2, 3, 5, and 6 according to the DIC and LPML values. However, the medians of

the DIC and LPML differences are close to 0 for both Models 4 since both $Z_1(s)$ and $Z_2(s)$ are correlated with the interaction term $Z_1(s)Z_2(s)$.

Figure 1: DIC and LPML Differences of Scenario 1



Furthermore, the intensity of DGM is $\lambda(s) = \lambda_0 \exp(\beta_1 \times Z_1^2(s))$, where $Z_1(s)$ is the x-coordinate. We choose $\lambda_0 = 50$ and $\beta_1 = 4$. We generate data on $[0, 1] \times [0, 1]$ and the average number of points over 100 replicates is 412. We compare the data generation model with three different models: Model 1: $\lambda(s) = \lambda_0 \exp(\beta_1 \times Z_1(s))$; Model 2: $\lambda(s) = \lambda_0 \exp(\beta_2 \times Z_2(s))$, where $Z_2(s)$ is the y-coordinate; Model 3: $\lambda(s) = \lambda_0 \exp(\beta_1 \times Z_1(s) + \beta_2 \times Z_2(s))$. We have the same prior distributions and same number of MCMC samples with scenario 1

The average DIC and LPML values and the selection percentage and model informations are shown in Table 3

Table 3: Selection Results of Scenario 2

Model	Average DIC	Average LPML	DIC Selection %	LPML Selection %
DGM	-4702.209	2351.101	94	94
Model 1	-4690.384	2345.186	6	6
Model 2	-4145.1794	2072.586	0	0
Model 3	-4689.554	2344.769	0	0

Furthermore, the medians and the inter quartile ranges (IQRs) of the DIC differences and the LPML differences are show in Table 4

Table 4: Median and inter quartile ranges (IQRs) of the DIC and the LPML differences for Scenario 2

	DIC	LPML
Model 1	10.729 (6.676,17.11)	-5.365 (-8.562, -3.335)
Model 2	551.8 (531.1,584.3)	-275.9 (-292.2, -1265.5)
Model 3	12.16 (7.26,17.83)	-6.079 (-8,941,-3.628)

From the results in Table 3 and Table 4, our proposed criteria can effectively select the true model and the difference of DIC and LPML between true model and candidate models is significant.

The intensity function of DGM in scenario 3 is $\lambda(s) = \exp(\beta_1 \times Z_1(s) + \beta_2 \times Z_2(s))$. $\mathbf{Z}_i, i = 1, \dots, 4$ are generated from Gaussian random fields based on R package **RandomFields**. Our choice of Gaussian random fields with mean 1 and the covariance with exponential kernel model with variance 1, scale parameter 1 and nugget variance 0.2. In this simulation we choose $\beta_1 = 2$, $\beta_2 = 1$, and $\lambda_0 = 1$ and generate data on $[0, 1] \times [0, 1]$. We have 100×100 grids on $[0, 1] \times [0, 1]$. Based on intensity surface on $[0, 1] \times [0, 1]$, we independently generate locations in each grids. We generate 100 data sets under this setting, and the average number of points in each data set is 544. We have the same prior distributions and the same number of MCMC samples with previous simulation. The average DIC and LPML values and the selection percentage are shown in Table 6. From this table, we see that the true model has the smallest DIC value, the largest LPML value, and the highest selection percentages according to both DIC and LPML.

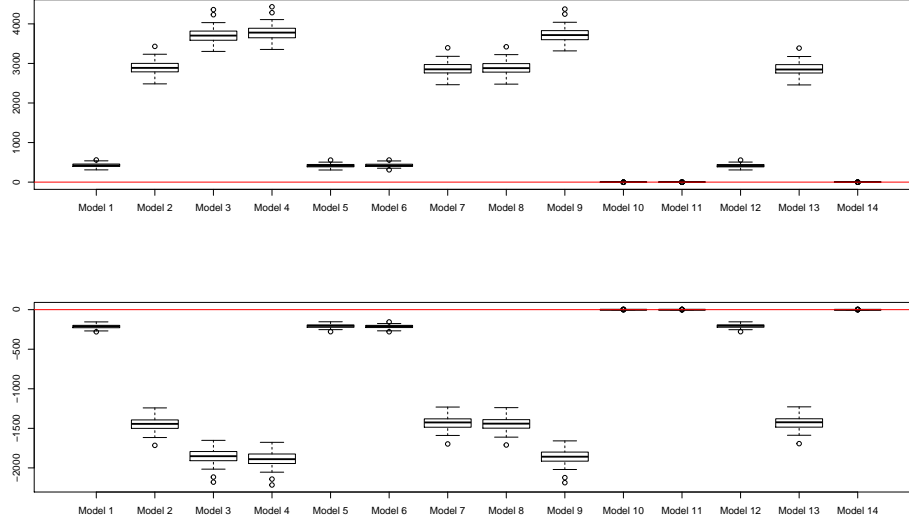
Furthermore, we also show the boxplots of the DIC difference and the LPML difference between the true model and each of the candidate models in Figure 2. The medians and the inter quartile ranges (IQRs) of the DIC differences in the top panel of Figure 2 are 1.608 (0.651, 2.012), 1.698 (0.826, 1.968), and 2.944 (1.492, 3.501) for Models 10, 11 and 14, respectively; and the medians and the inter quartile ranges (IQRs) of the LPML differences in the bottom panel of Figure 2 are -0.805 (-0.412, -0.985), -0.849 (-0.412, -0.985), and -1.475

Table 5: Selection Results of Scenario 3

Model	Average DIC	Average LPML	DIC Selection %	LPML Selection %
Model 1 (β_1)	-8877.358	4438.677	0	0
Model 2 (β_2)	-6402.960	3201.478	0	0
Model 3 (β_3)	-5590.344	2795.170	0	0
Model 4 (β_4)	-5521.848	2760.921	0	0
DGM (β_1, β_2)	-9303.699	4651.845	74	74
Model 5 (β_1, β_3)	-8890.624	4445.308	0	0
Model 6 (β_1, β_4)	-8879.830	4439.910	0	0
Model 7 (β_2, β_3)	-6439.253	3219.623	0	0
Model 8 (β_2, β_4)	-6409.395	3204.694	0	0
Model 9 (β_3, β_4)	-5577.677	2788.834	0	0
Model 10 ($\beta_1, \beta_2, \beta_3$)	-9302.598	4651.292	15	15
Model 11 ($\beta_1, \beta_2, \beta_4$)	-9302.500	4651.243	9	9
Model 12 ($\beta_1, \beta_3, \beta_4$)	-8891.348	4445.667	0	0
Model 13 ($\beta_2, \beta_3, \beta_4$)	-6443.625	3221.808	0	0
Model 14 ($\beta_1, \beta_2, \beta_3, \beta_4$)	-9301.493	4650.738	2	2

(-0.754, -1.758) for Models 10, 11 and 14, respectively. Unlike scenario 3, the whole boxes of the DIC differences are above 0 while the boxes of the LPML differences are below 0. Thus, there is an overwhelming evidence in favor of the true model according both DIC and LPML.

Figure 2: DIC and LPML Differences of Scenario 3



Finally, the intensity of DGM of scenario 4 is $\lambda(s) = \exp(\beta_1 \times Z_1(s) + \beta_2 \times Z_2(s) + W(s))$, $Z_i, i = 1, \dots, 3$ are generated from uniform distribution $U(0, 1)$. $W(s)$ is generated from Gaussian random with mean 0 and the covariance with exponential kernel model with variance 1, scale parameter 1 and nugget variance 0.2, which is unobserved in this simulation. In this simulation we choose $\beta_1 = 4$, $\beta_2 = 4$, and $\lambda_0 = 1$ and generate data on $[0, 1] \times [0, 1]$. We generate 100 data sets under this setting, and the average number of points in each data set is 182. The full model is this simulation is $\lambda(s) = \exp(\beta_1 \times Z_1(s) + \beta_2 \times Z_2(s) + \beta_3 \times Z_3(s))$. We have 100×100 grids on $[0, 1] \times [0, 1]$. Based on intensity surface on $[0, 1] \times [0, 1]$, we independently generate locations in each grids. We have the same prior distributions and same number of MCMC samples with previous scenarios. The average DIC and LPML values and the selection percentage are shown in Table 6. From this table, we see that the true model has the smallest DIC value, the largest LPML value, and the highest selection percentages according to both DIC and LPML. From this table, we see that the true model has the smallest DIC value, the largest LPML value, and the highest selection percentages according to both DIC and LPML.

Table 6: Selection Results of Scenario 4

Model	Average DIC	Average LPML	DIC Selection %	LPML Selection %
Model 1 (β_1)	-1694.704	847.344	0	0
Model 2 (β_2)	-1696.554	848.269	0	0
Model 3 (β_3)	-1459.131	729.560	0	0
DGM (β_1, β_2)	-1873.874	936.921	88	88
Model 4 (β_1, β_3)	-1693.393	846.683	0	0
Model 5 (β_2, β_3)	-1695.379	847.676	0	0
Model 6 ($\beta_1, \beta_2, \beta_3$)	-1872.952	936.454	12	12

5 Real Data Analysis

5.1 USGS Earthquake Data

The earthquake data from USGS, the Earthquake Hazards Program of United States Geological Survey (USGS), can be accessed via <https://earthquake.usgs.gov/earthquakes/>. The data set we consider is composed of conterminous U.S. earthquakes which have magnitude over 2.5 from 10-30-2018 to 11-27-2018. From USGS, conterminous U.S. refers to a rectangular region including the lower 48 states and surrounding areas which are outside the Conterminous U.S.. The total number of earthquakes is 155. The map of the locations of earthquakes is shown in Figure 3. In order to properly examine the relationship of these locations, we transform the latitude and the longitude of the earthquakes to UTM (Universal Transverse Mercator) coordinate system and then scale UTM coordinate system to a $[0, 1] \times [0, 1]$ square. The locations of earthquakes in a unit square are shown in Figure 4. The spatial covariates used in this analysis include x -coordinates which are transferred by longitudes, y -coordinates which are transferred by latitudes, and the distance to New Madrid Seismic Zone (Tuttle et al., 2005) which has coordinates (36.58 N, 89.58 W). Similarly, we transform the latitude and the longitude of the New Madrid Seismic Zone to UTM system and scale it to the same unit square. New Madrid Seismic Zone is a major seismic zone and a prolific source of intraplate earthquakes in the southern and midwestern United States.

Figure 3: Map of Locations of the Earthquake

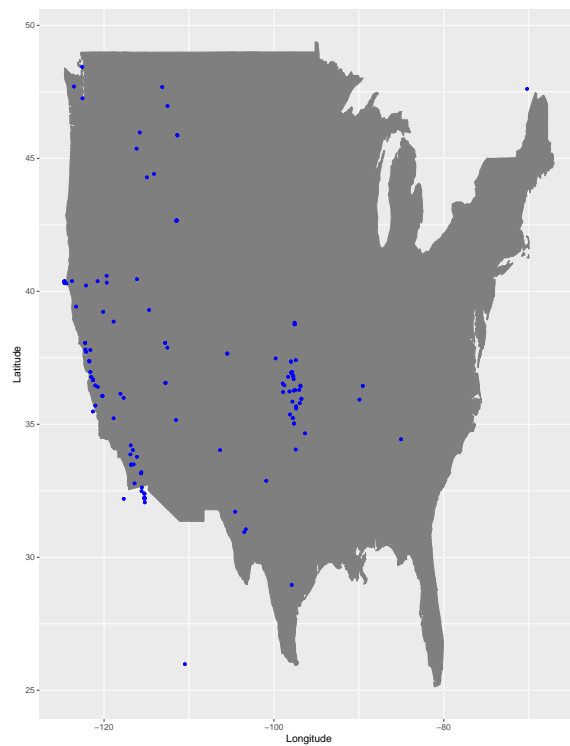
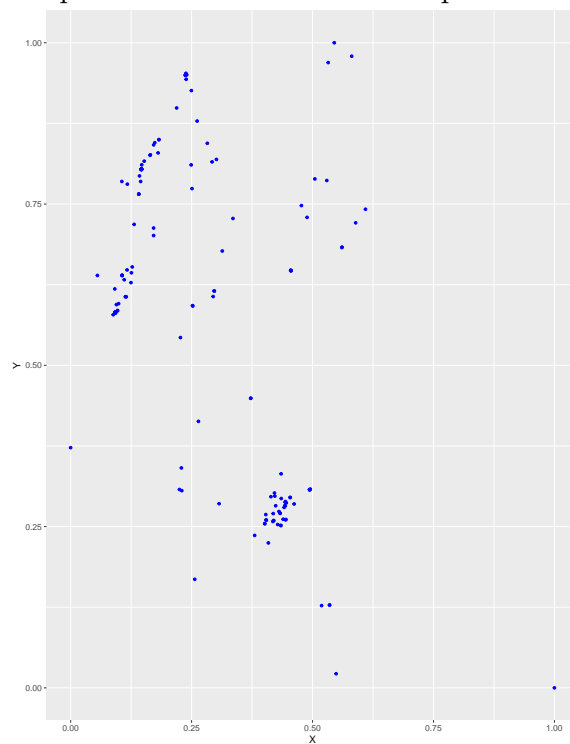


Figure 4: Map of Locations of the Earthquake in Unit Square



The full spatial intensity model for the spatial point process is given by

$$\lambda(s) = \lambda_0 \exp(\beta_1 Z_1(s) + \beta_2 Z_2(s) + \beta_3 Z_3(s)), \quad (20)$$

where $Z_1(s)$ is x -coordinate, $Z_2(s)$ is y -coordinate, and $Z_3(s)$ is the distance to the New Madrid Seismic Zone. Including the homogeneous spatial Poisson process model, we have 8 candidate models. With the thinning interval to be 10, 2,000 samples are kept for calculation after a burn-in of 30,000 samples using NIMBLE in R for each models. The prior for β s is $N(0, 10^2)$ and the prior for λ_0 is $G(1, 1)$. The DIC and LPML values of these 8 candidate models are given in Table 7. The DIC and LPML values in Table 7 suggest that the model

Table 7: DIC and LPML of Earthquake Data

Model	DIC	LPML	Model	DIC	LPML
$\beta_1, \beta_2, \beta_3$	-1268.687	634.329	β_1, β_2	-1261.741	630.864
β_1, β_3	-1239.627	619.8027	β_2, β_3	-1218.654	609.317
β_1	-1179.762	589.878	β_2	-1219.484	609.7372
β_3	-1206.92	603.452	Homogenous	-1192.528	596.262

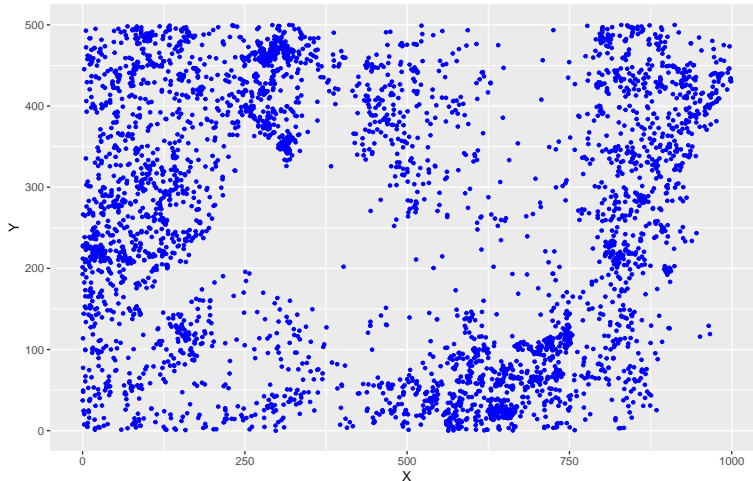
with $\beta_1, \beta_2, \beta_3$ is the best. The posterior means, the posterior standard deviations and the 95% highest posterior density (HPD) intervals (Chen & Shao, 1999) under the best model are reported in Table 8. From Table 8, we see that the occurrence of earthquake has a higher

Table 8: Best Model Parameter Estimation of Earthquake Data

Parameter	Posterior Mean	Posterior Standard Deviation	HPD interval
β_1	-1.975	0.352	$(-2.699, -1.343)$
β_2	5.721	1.161	$(3.621, 7.884)$
β_3	-2.744	1.213	$(-4.909, -0.512)$
λ_0	37.850	5.491	$(28.314, 49.394)$

intensity around the New Madrid Seismic Zone and the southwestern area of U.S., which is consistent with the findings in the literature (Fuller, 1988).

Figure 5: Locations Map of *B.pendula*



5.2 Forest of Barro Colorado Island (BCI)

BCI data have been analyzed in the literature (Leininger et al., 2017; Thurman et al., 2015; Yue & Loh, 2015; Thurman & Zhu, 2014). The data are obtained from a long-term ecological monitoring program, which contains 400,000 individual trees since the 1980s at the Barro Colorado Island (BCI) in central Panama (Hubbell et al., 1999; Condit, 1998; Condit et al., 2012). We choose the same species like (Thurman & Zhu, 2014) in our data analysis. We model the intensity of the *B.pendula* trees as a log-linear function of the incidences of six other tree species (*Eugenia nesiotica*, *Eugenia oerstediana*, *Piper cordulatum*, *Protium panamense*, *Sorocea affinis*, and *Talisia croatii*). The map of the locations of *B.pendula* trees mentioned above is shown in Figure 5.2.

We choose three different pixel resolutions, $5m \times 5m$, $10m \times 10m$, and $20m \times 20m$ for the incidences of six other tree species (6 spatial covariates). The full spatial intensity model for the spatial point process is given by

$$\lambda(s) = \lambda_0 \exp(\beta_1 Z_1(s) + \cdots + \beta_6 Z_6(s)), \quad (21)$$

where $Z_i(s)$ is the i -th species's pixel value on location s . Including the homogeneous spatial Poisson process model, we have 64 candidate models. 8,000 samples are kept for calculation after a burn-in of 10,000 samples using NIMBLE in R for each model. The prior for β s is $N(0, 10^2)$ and the prior for λ_0 is $G(1, 1)$. The DIC and the LPML values of the best models

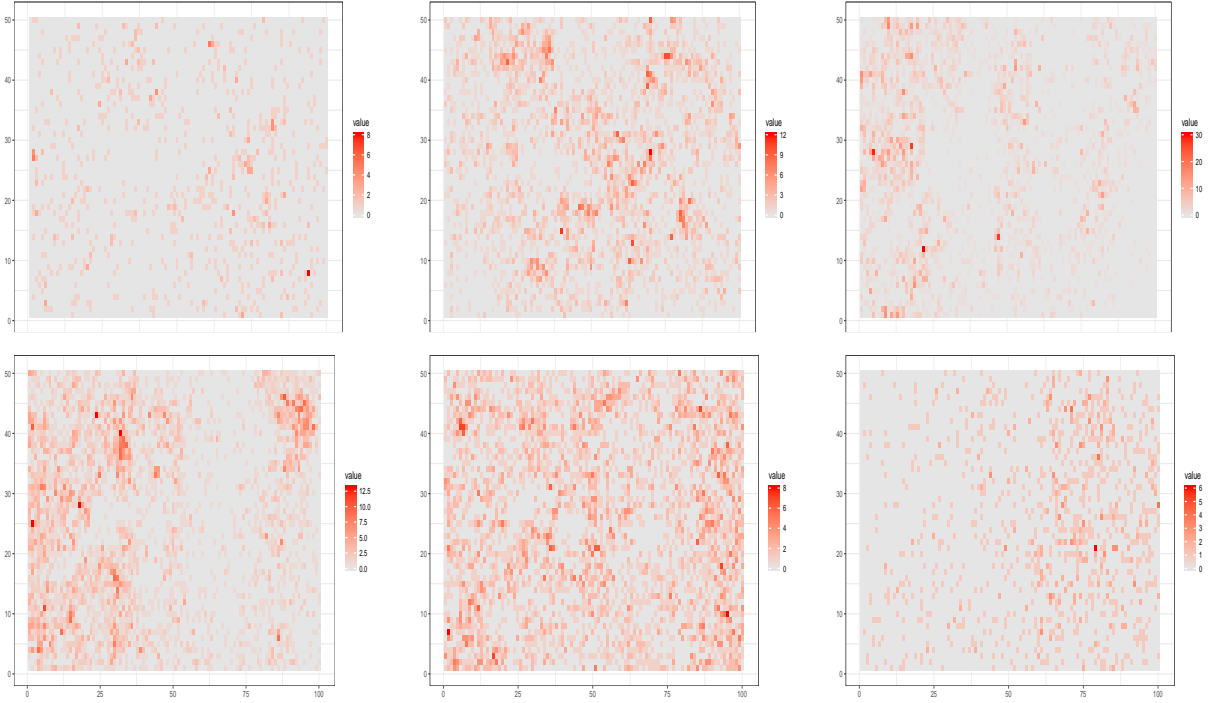
for the three pixel resolutions are given in Table 9.

Table 9: Model Comparison for Different Pixel Resolutions

Pixel Resolution	Best Model	DIC	LPML
$5m \times 5m$	(β_4, β_5)	-57521.48	28760.74
$10m \times 10m$	$(\beta_1, \beta_3, \beta_4, \beta_5)$	-58255.15	29127.57
$20m \times 20m$	$(\beta_3, \beta_4, \beta_5)$	-58188.46	29094.22

The combination of the covariate model and the resolution with the smallest DIC value and the largest LPML value is the model with $(\beta_1, \beta_3, \beta_4, \beta_5)$ plus the $10m \times 10m$ resolution. The posterior means, the posterior standard deviations and the 95% HPD intervals under this best combined covariate model and resolution are reported in Table 10. Figure 6 shows the plots of 6 different species in the $10m \times 10m$ pixel resolution.

Figure 6: $10m \times 10m$ Pixel Resolution Covariates Map (Red indicate larger values)



From Table 10, we see that (i) the *B.pendula* trees seem to be attracted to *Eugenia oerstediana*, *Piper cordulatum*, *Protium panamense*, and *Sorocea affinis*; and (ii) *Eugenia nesiotica* and *Talisia croatii* have no effects on *B.pendula* trees.

Table 10: Posterior Estimation Results of BCI Data

Parameter	Posterior Mean	Posterior SD	95%HPD interval
β_1	0.2986	0.0275	(0.2415,0.3511)
β_3	0.1083	0.0037	(0.1013,0.1156)
β_4	0.2305	0.0064	(0.2180,0.2420)
β_5	0.2825	0.0122	(0.2595,0.3053)
λ_0	1200.4259	25.3233	(1157.8434,1254.6554)

6 Discussion

In this paper, we have developed the Bayesian parameter estimation and model selection in Poisson point process models in regression context. Our simulation results indicate that our proposed method is more likely to select the correct model and obtain the estimators that are closer to the true values if we had fit the true model. Like most model selection methods, our proposed method needs calculating DIC and LPML for all candidate models. Developing a computational algorithm as in (Chen, Huang, Ibrahim, & Kim, 2008) is an important future work. In addition, extending our proposed criterion to a more complicated spatial point process like Gibbs point process (Moller & Waagepetersen, 2007) should be a natural extension of our work. Furthermore, another future work is to investigate the theoretical properties of the proposed procedure like (Li, Jun, & Zeng, 2017). Moreover, the development of the predictive distribution-based criterion like WAIC (Vehtari, Gelman, & Gabry, 2017) or the L-measure (Ibrahim, Chen, & Sinha, 2001) for spatial point process is another interesting future work.

Acknowledgement

Dr. Chen’s research was partially supported by NIH grants #GM70335 and #P01CA142538. Dr. Hu’s research was supported by Dean’s office of College of Liberal Arts and Sciences in University of Connecticut.

References

- Akaike, H. (1974). A new look at the statistical model identification. *IEEE transactions on automatic control*, 19(6), 716–723.
- Banerjee, S., Carlin, B. P., & Gelfand, A. E. (2014). *Hierarchical modeling and analysis for spatial data*. Crc Press.
- Beale, C. M., Lennon, J. J., Yearsley, J. M., Brewer, M. J., & Elston, D. A. (2010). Regression analysis of spatial data. *Ecology letters*, 13(2), 246–264.
- Chen, M.-H., Huang, L., Ibrahim, J. G., & Kim, S. (2008). Bayesian variable selection and computation for generalized linear models with conjugate priors. *Bayesian analysis (Online)*, 3(3), 585.
- Chen, M.-H., & Shao, Q.-M. (1999). Monte carlo estimation of bayesian credible and hpd intervals. *Journal of Computational and Graphical Statistics*, 8(1), 69–92.
- Chen, M.-H., Shao, Q.-M., & Ibrahim, J. G. (2012). *Monte carlo methods in bayesian computation*. Springer Science & Business Media.
- Condit, R. (1998). *Tropical forest census plots: methods and results from barro colorado island, panama and a comparison with other plots*. Springer Science & Business Media.
- Condit, R., Lao, S., Pérez, R., Dolins, S. B., Foster, R., & Hubbell, S. (2012). [dataset:] barro colorado forest census plot data (version 2012).
- Cressie, N. A. (1993). *Statistics for spatial data*. Wiley Online Library.
- de Valpine, P., Turek, D., Paciorek, C. J., Anderson-Bergman, C., Lang, D. T., & Bodik, R. (2017). Programming with models: Writing statistical algorithms for general model structures with NIMBLE. *Journal of Computational and Graphical Statistics*, 26(2), 403–413.
- Diggle, P. J. (2013). *Statistical analysis of spatial and spatio-temporal point patterns*. CRC Press.
- Fuller, M. L. (1988). *The new madrid earthquake* (Vol. 494). Central United States Earthquake Consortium.
- Gelfand, A. E., & Dey, D. K. (1994). Bayesian model choice: asymptotics and exact calculations. *Journal of the Royal Statistical Society. Series B (Methodological)*, 501–

- Hoerl, A. E., & Kennard, R. W. (1970). Ridge regression: Biased estimation for nonorthogonal problems. *Technometrics*, *12*(1), 55–67.
- Hubbell, S. P., Foster, R. B., O'Brien, S. T., Harms, K. E., Condit, R., Wechsler, B., ... De Lao, S. L. (1999). Light-gap disturbances, recruitment limitation, and tree diversity in a neotropical forest. *Science*, *283*(5401), 554–557.
- Ibrahim, J. G., Chen, M.-H., & Sinha, D. (2001). Criterion-based methods for bayesian model assessment. *Statistica Sinica*, 419–443.
- Ishwaran, H., Rao, J. S., et al. (2005). Spike and slab variable selection: frequentist and bayesian strategies. *The Annals of Statistics*, *33*(2), 730–773.
- Leininger, T. J., Gelfand, A. E., et al. (2017). Bayesian inference and model assessment for spatial point patterns using posterior predictive samples. *Bayesian Analysis*, *12*(1), 1–30.
- Li, Y., Jun, Y., & Zeng, T. (2017). Deviance information criterion for bayesian model selection: Justification and variation.
- Moller, J., & Waagepetersen, R. P. (2003). *Statistical inference and simulation for spatial point processes*. CRC Press.
- Moller, J., & Waagepetersen, R. P. (2007). Modern statistics for spatial point processes. *Scandinavian Journal of Statistics*, *34*(4), 643–684.
- Polson, N. G., & Scott, J. G. (2010). Shrink globally, act locally: Sparse bayesian regularization and prediction. *Bayesian statistics*, *9*, 501–538.
- Reich, B. J., Fuentes, M., Herring, A. H., & Evenson, K. R. (2010). Bayesian variable selection for multivariate spatially varying coefficient regression. *Biometrics*, *66*(3), 772–782.
- Schwarz, G., et al. (1978). Estimating the dimension of a model. *The annals of statistics*, *6*(2), 461–464.
- Spiegelhalter, D. J., Best, N. G., Carlin, B. P., & Van Der Linde, A. (2002). Bayesian measures of model complexity and fit. *Journal of the Royal Statistical Society: Series B (Statistical Methodology)*, *64*(4), 583–639.
- Thurman, A. L., Fu, R., Guan, Y., & Zhu, J. (2015). Regularized estimating equations for

- model selection of clustered spatial point processes. *Statistica Sinica*, 173–188.
- Thurman, A. L., & Zhu, J. (2014). Variable selection for spatial poisson point processes via a regularization method. *Statistical Methodology*, 17, 113–125.
- Tibshirani, R. (1996). Regression shrinkage and selection via the lasso. *Journal of the Royal Statistical Society. Series B (Methodological)*, 267–288.
- Tuttle, M. P., Schweig, E. S., Campbell, J., Thomas, P. M., Sims, J. D., & Lafferty, R. H. (2005). Evidence for new madrid earthquakes in ad 300 and 2350 bc. *Seismological Research Letters*, 76(4), 489–501.
- Vehtari, A., Gelman, A., & Gabry, J. (2017). Practical bayesian model evaluation using leave-one-out cross-validation and waic. *Statistics and Computing*, 27(5), 1413–1432.
- Waagepetersen, R. (2004). Convergence of posteriors for discretized log gaussian cox processes. *Statistics & Probability Letters*, 66(3), 229–235.
- Wang, H., & Zhu, J. (2009). Variable selection in spatial regression via penalized least squares. *Canadian Journal of Statistics*, 37(4), 607–624.
- Yue, Y., & Loh, J. M. (2015). Variable selection for inhomogeneous spatial point process models. *Canadian Journal of Statistics*, 43(2), 288–305.
- Zou, H., & Hastie, T. (2005). Regularization and variable selection via the elastic net. *Journal of the Royal Statistical Society: Series B (Statistical Methodology)*, 67(2), 301–320.